physica status solidi rrl
www.pss-rapid.com

Pressure-Induced Isostructural Phase Transition in Biskyrmion Host Hexagonal MnNiGa

*Anupam K. Singh, Parul Devi, Ajit K. Jena, Ujjawal Modanwal, Seung-Cheol Lee, Satadeep Bhattacharjee, Boby Joseph, and Sanjay Singh**

Magnetic skyrmions are vortex-like spin textures, which can be manipulated by external stress or pressure via magnetoelastic effects. Herein, the observation of isostructural phase transition in a biskyrmion host hexagonal MnNiGa at pressure $P \approx 4$ GPa using pressure-dependent synchrotron X-Ray powder diffraction (XRD) data analysis is presented. The XRD data reveals anisotropic compression behavior with pressure with different compression rates of the *a*-axis in the basal plane and the *c*-axis in the prismatic plane. However, the hexagonal symmetry remains unchanged for pressure up to 14 GPa. Fitting of unit cell volume with pressure using a second-order Birch–Murnaghan equation of state reveals that the data fall into two distinct curves for those above and below 4 GPa. Herein, the understanding of crystal structure with the application of hydrostatic pressure in the biskyrmion host MnNiGa is contributed to, wherein the skyrmion textures can be manipulated by pressure due to their magnetoelastic character.

1. Introduction

Magnetic skyrmions are a kind of spin textures wherein particle-type swirling of spins around the unit sphere takes place in the nanometer length scale.[1,2] They have been the subject of tremendous interest in recent years due to their developing potentiality in high-density information carriers, data processing, and memory devices[3–7] owned by their unique properties such as nanometer size, topological stability, and low power consumption (low current density $\approx 10^5$–10^6 A m^{-2}) required to drive the skyrmion textures.[8–11] Among a various types of existing skyrmion textures,[2] biskyrmions received a great deal of attention in recent years due to their size and topological charge tunability using the thickness, magnetic field, and electrical current.[12] Biskyrmions are a set of two individual skyrmions with opposite helicities (or vorticity).[13] In general, biskyrmions have been observed in the centrosymmetric materials having strong uniaxial magnetic anisotropy, for example, $La_{2-2x}Sr_{1+2x}Mn_2O_7$,[13] MnNiGa,[14] and MnPdGa.[12]

Among different biskyrmion hosting materials, hexagonal MnNiGa turns out to be a most important candidate as it exhibits superstable biskyrmion textures in the wide temperature range (16–340 K)[14,15] with a high value of ferromagnetic (FM) transition temperature $T_C \approx 350$ K.[14–16] The present alloy system (MnNiGa) requires a comparatively low magnetic field (≈0.25 T) to induce the biskyrmion textures at room temperature and can be stabilized even at zero magnetic field using field cooling protocols.[14,15] MnNiGa exhibits a uniaxial magnetic easy axis along the *c*-direction below the FM T_C. Apart from T_C, an interesting spin reorientation transition (SRT), below which antiferromagnetic (AFM) components appear in the basal plane, has been observed in MnNiGa.[16] The magnetic properties of MnNiGa can be easily modified by compositional tuning.[16] A recent theoretical study proposed that the magnetism is dominated by the shortest Mn–Mn distance with competing FM and AFM interactions along *c*-axis in MnNiGa.[17] In MnNiGa, a magnetically originated anomaly in the *c*/*a* ratio has been reported without any crystallographic symmetry change at SRT.[16] Such an anomaly in structural parameters at magnetic transition with preserved crystallographic symmetry is the indication of the presence of magnetoelastic effects[18] or isostructural phase transitions.[18,19] The magnetoelastic effects provide the understanding of spin-lattice coupling.[18] The magnetoelastic effect has been reported in the skyrmions hosting B20 chiral magnets using Landau–Ginzburg free energy functional formulation.[20,21] The stability of spin textures of skyrmion is very sensitive to external uniaxial stress or pressure, which can manipulate the stability of these spin textures through intrinsic spin-lattice coupling.[22–24] Therefore, manipulation of skyrmions with external parameter like pressure is of great importance to improve

A. K. Singh, U. Modanwal, S. Singh
School of Materials Science and Technology
Indian Institute of Technology (Banaras Hindu University)
Varanasi 221005, India
E-mail: ssingh.mst@iitbhu.ac.in

P. Devi
Dresden High Magnetic Field Laboratory
Helmholtz-Zentrum Dresden – Rossendorf
Bautzner Landstr. 400, 01328 Dresden, Germany

A. K. Jena, S.-C. Lee, S. Bhattacharjee
Indo-Korea Science and Technology Center (IKST)
Bangalore 560065, India

B. Joseph
Elettra-Sincrotrone Trieste
Strada Statale 14, Km 163.5 in Area Science Park, Basovizza 34149, Italy

The ORCID identification number(s) for the author(s) of this article can be found under https://doi.org/10.1002/pssr.202200057.

DOI: 10.1002/pssr.202200057

their practical applicability.[25–27] Although the stability of skyrmions by pressure-tuning has been investigated in the noncentrosymmetric materials, for example, MnSi,[26] FeGe,[27] Cu_2OSeO_3,[25,28] there is almost negligible report in the centrosymmetric materials like biskyrmion host MnNiGa. This calls for a detailed study on the pressure-tuning of biskyrmions in the centrosymmetric MnNiGa.

Isostructural phase transition induced by pressure is an interesting phenomenon wherein the anomaly in structural parameters like lattice parameter, c/a ratio, or volume collapse appears without any change of the crystallographic symmetry.[18,29–31] Such phase transitions always received significant attention as they are very seldom. In general, the isostructural phase transition is associated with the change in electronic structure, which reveals anomalies in the frequency of associated phonon mode.[30,31] The electronic structure can be easily modified with pressure, which may lead to significant changes in isostructural phase transitions.[30,31]

In MnNiGa, the maximum density of biskyrmions has been reported[14] at $T_{SRT} \approx 200$ K, where AFM components increase significantly due to spin canting.[16] The application of hydrostatic pressure at room temperature can compress the lattice and result into the reduced Mn–Mn interatomic distances, which may lead to the modification of magnetic interactions in MnNiGa as observed in skyrmion host Cu_2OSeO_3.[28] In addition, increasing behavior of FM T_C with hydrostatic pressure (increasing rate of $dT_C/dP \approx 1.7$ K kbar^{-1})[32] has been reported for a similar hexagonal sister compound MnPtGa, which hosts skyrmions with maximum stability at its $T_{SRT} \approx 215$ K.[33] Therefore, a natural question arises that whether the SRT can be induced at room temperature driven by external pressure via modification in the magnetic interaction in MnNiGa. The answer will be helpful to stabilize the maximum density of biskyrmions at room temperature in MnNiGa and lead to low power consumption in the spintronic devices.[16] Further, the skyrmion host Cu_2OSeO_3 revealed dramatic enhancement in the temperature window of stable skyrmions driven by external pressure and also shows interesting pressure-driven phase transitions.[28] Therefore, a detailed pressure study of MnNiGa is required to explore the stability of biskyrmions and crystal structure under external hydrostatic pressure.

We present the observation of the pressure-driven isostructural phase transition in MnNiGa magnet using in situ high-pressure synchrotron XRD data analysis. The high-pressure XRD data analysis up to 14 GPa reveals the continuous reduction of lattice parameters with nonlinearity above 4 GPa. The different compression rates of the a-axis in the basal plane and the c-axis in the prismatic plane indicate the anisotropic compression behavior. However, the hexagonal symmetry remains unchanged with pressure; the fitting of lattice volume with pressure using second-order Birch–Murnaghan (B–M) equation of state reveals an isostructural phase transition at $P \approx 4$ GPa. The present results provide the understanding of the crystal structure of biskyrmion host MnNiGa with the application of hydrostatic pressure.

2. Results and Discussion

2.1. Phase Purity and Phase Transition

The Rietveld refinement using the XRD data at ambient condition is shown in **Figure 1**a, which shows an excellent fit between observed and calculated profiles by accounting for all the Bragg peaks. This confirms that the MnNiGa crystallizes into the hexagonal structure with $P6_3/mmc$ space group. The refined lattice parameters were found to be $a = b = 4.1574(1)$ Å, $c = 5.3261(1)$ Å. The present diffraction pattern and refined lattice parameters are in good agreement with the previous report.[14,16] Thus, XRD data at ambient conditions confirm the phase purity of the MnNiGa sample.

The temperature dependence of the real part of AC susceptibility ($\chi'(T)$) is shown in Figure 1b. On lowering the temperature, the sudden increase in $\chi'(T)$ around 350 K corresponds to the paramagnetic phase to FM phase transition. The value of FM $T_C \approx 347$ K was determined by taking minima of first-order differentiation of $\chi'(T)$. In addition to FM T_C, the $\chi'(T)$

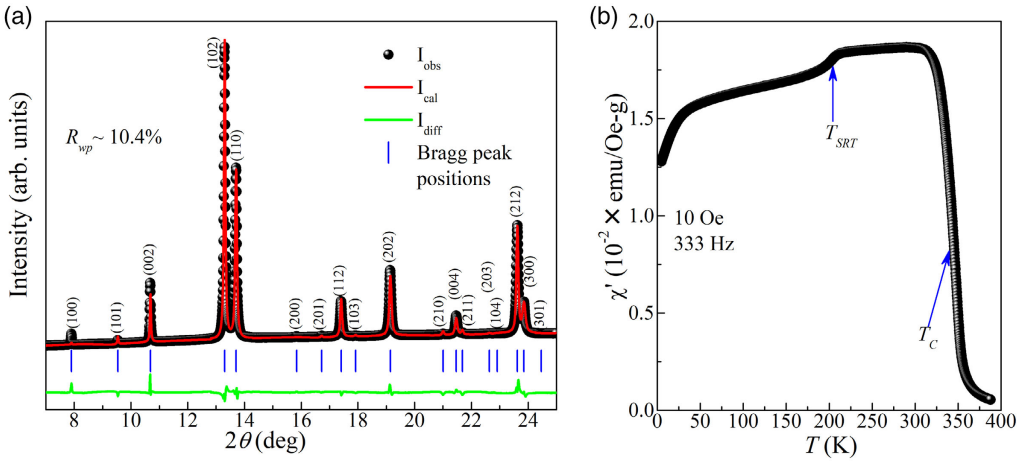

Figure 1. a) Result of Rietveld refinement using synchrotron X-Ray powder diffraction pattern at the ambient condition of MnNiGa. The "R_{wp}" represents the weighted agreement factor of refinement. The miller indices are given above each reflection. b) Temperature dependence of real part of AC susceptibility (χ') of MnNiGa. The "T_C" and "T_{SRT}" indicate ferromagnetic and spin reorientation transition temperatures, respectively.

decreases gradually below 200 K (see Figure 1b) due to the presence of SRT.[16] The SRT temperature was found at $T_{SRT} \approx 200$ K as calculated by the temperature derivative of $\chi'(T)$. However, a rapid decrease in $\chi'(T)$ can be noted below 50 K, which is a matter of future investigation. The present behavior of $\chi'(T)$ and magnetic transition temperatures are in good agreement with the previous report.[16]

2.2. Structural Investigation under Hydrostatic Pressure

The XRD pattern at different pressure is shown in **Figure 2**a, whose enlarged view around the most intense Bragg peak region is depicted in Figure 2b. In Figure 2, the absence of any splitting or appearance of additional Bragg peaks with pressure manifests that the hexagonal symmetry remains preserved. This indicates the absence of any structure phase transition in MnNiGa with pressure up to 14 GPa, the maximum pressure up to which data has been collected.

Further, the systematic shifting of the Bragg peaks to the higher 2θ side with pressure suggests the compression of lattice parameters or interplanar spacings (see Figure 2). It is important to mention here that, however, the intensity of (110) reflection should be higher than (102) as observed in the computed diffraction pattern, the reverse situation at the ambient condition (see Figure 1a) as well as at lower pressure (see Figure 2b) is certainly due to texturing effect. At $P \geq 3.96$ GPa, the intensity of (110) reflection became higher than (102) reflection (intensity switching), which suggests the texturing effect is suppressed at higher pressure (see Figure 2b). All these behaviors in the data is found to be reversible with pressure, as demonstrated by a comparison of the bottom XRD pattern, which was collected at 0.22 GPa during pressure application, and the top XRD pattern, which was collected at 0.5 GPa during pressure release (see Figure 2b). This indicates reversibility of structure with the pressure effects, that is, after releasing the pressure, complete recovery of the structure to the ambient conditions. This reversibility behavior with pressure in MnNiGa is in marked contrast to other skyrmion host Cu_2OSeO_3, wherein the irreversibility behavior with pressure has been observed.[28] The reversibility behavior of MnNiGa makes this alloy system ideal for pressure-tuning of skyrmion textures.

The lattice parameters are obtained from the Rietveld refinement using high-pressure XRD data. The evolution of lattice parameters (a and c) with pressure is shown in **Figure 3**a,b. However, the behavior of lattice parameter at low pressure shows linear compression as indicated by a linear fit to the observed lattice parameter, a clear departure from the linearity observed above 4 GPa in the form of deviation between extrapolated linear fit and the data in Figure 3a,b. The slope of linear fit to in-plane (a) and out-of-plane (c) lattice parameter was found to be $da/dP \approx -0.01126$ Å GPa^{-1} and $dc/dP \approx -0.02306$ Å GPa^{-1}, respectively (see Figure 3a,b). This means a higher compression rate for the out-of-plane c-axis in comparison to the in-plane a-axis with pressure, that is, presence of anisotropic compression behavior in the MnNiGa as reported in the other hexagonal system.[30]

In addition to the lattice parameters, the deviation from the systematic linearity with pressure above 4 GPa was also observed in the unit cell volume (V) and c/a ratio as depicted in **Figure 4** and in the inset of Figure 4, respectively. It is important to mention here that we have a large number of data points at both

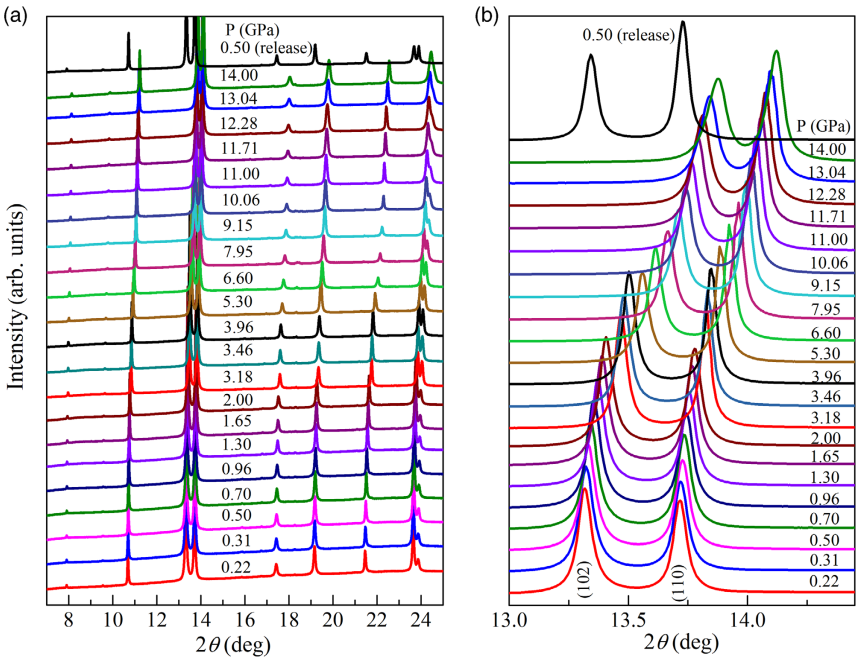

Figure 2. a) The synchrotron X-Ray powder diffraction patterns collected at various pressure (indicated) up to 14 GPa of MnNiGa. b) The enlarged view of (a) around the most intense Bragg peak region. The miller indices of both major peaks are given in the bottom most in (b). The "P (GPa)" represents the pressure in the GPa unit. The top most pattern labeled by "0.50 (release)," was collected during releasing the pressure with effective pressure of 0.50 GPa.

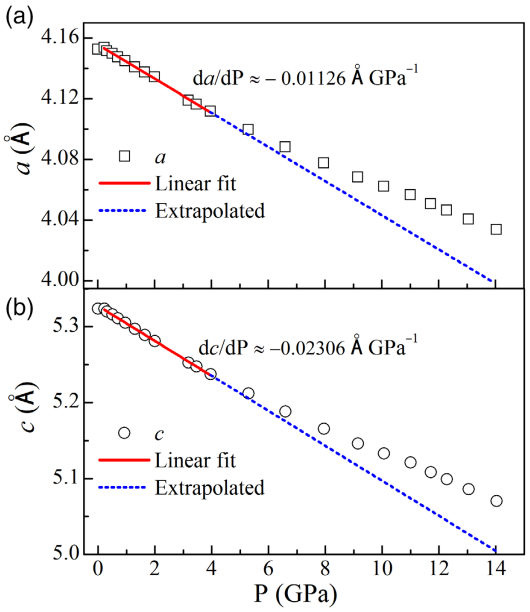

Figure 3. Pressure dependence of a) in-plane and b) out-of-plane lattice parameters of MnNiGa. The red line and dotted blue line in (a) and (b) represent the linear compression and extrapolated region of linear compression behavior, respectively. The "da/dP" and "dc/dP" indicate the linear compression rate in the a and c parameter in (a) and (b), respectively. The error in lattice parameters is smaller than the symbol size.

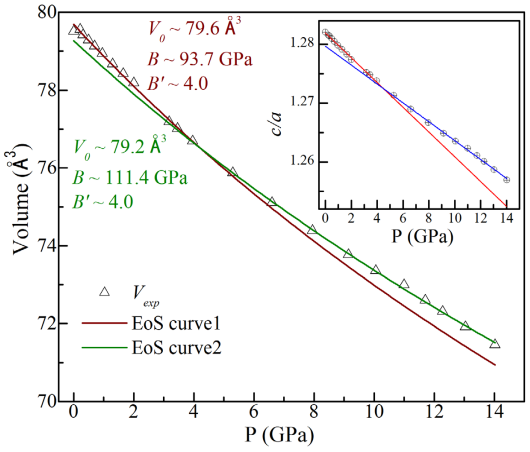

Figure 4. Pressure dependence of unit cell volume of MnNiGa. Solid lines indicate the results of a second-order Birch–Murnaghan equation-of-state (B–M EoS) fit to the data. "EoS1" and "EoS2" represent the fitting considering the data up to 4 GPa and above 4 GPa, respectively. The V_0, B, and B' are the parameters obtained from the fit. Pressure dependence of the c/a ratio is depicted in the inset, wherein red and straight blue lines indicate the plot from lower to higher and higher- to lower-pressure region, respectively.

low- and high-pressure regions, therefore such kind of detailed analysis (i.e., reliable slope change in the c/a ratio) is possible. The decreasing behavior of the c/a ratio with pressure further manifests that the c-axis is more compressible than the a-axis (see the inset of Figure 4). This behavior is usually expected for anisotropic crystals due to the weak van der Waals interlayer forces along the c-direction.[30]

The significant deviation in the structural parameters (a, c, c/a, and V) above 4 GPa from the linearity without any change in symmetry is the indication of isostructural phase transition.[30,31,34–38] To investigate it, a second-order B–M EoS[39,40] (2nd O B–M EoS) was employed to model the evolution of volume with pressure (P–V). Since considering the whole P–V region together did not yield a satisfactory fit, two separate regions of the P–V plot were considered for the fitting using two independent 2nd O B–M EoS.[41] The first region was considered at the lower-pressure side (up to 4 GPa), while the second was at the higher-pressure side (above 4 GPa). The result of the fitting is shown in Figure 4, which yield different bulk modulus (B) for different region. The value of B was found to be increased from ≈93.7 to ≈111.4 GPa from low- to high-pressure regions. In skyrmion host Cu_2OSeO_3, cubic to monoclinic phase transition has been observed at 7 GPa with B increased from 74.8 to 161.1 GPa.[28] Comparing to this, a relatively smaller change in B (≈93.7 to ≈111.4 GPa) of MnNiGa manifests the pressure-induced isostructural phase transition above 4 GPa and suggests that the high-pressure phase has lesser compressibility than low-pressure phase in MnNiGa as reported in other systems (like PdPS[34]). The anomaly above 4 GPa is also observed in the linearization of B–M EoS with the Eulerian strain[42,43] (see Figure S1, Supporting Information and related texts on page 1 of the Supporting Information). Interestingly, our theoretical results (electronic band structure, density of states at the Fermi level and bulk modulus) are found to be in excellent agreements with the experimental findings (see Figure S2, S3, Supporting Information and related texts on pages 2 to 3 of the Supporting Information). The presence of pressure-induced isostructural phase transition is of fundamental importance and opens a new pathway for future investigation of pressure-tuning of skyrmion textures in the centrosymmetric MnNiGa and related systems.

The maximum density of biskyrmions has been reported at $T_{SRT} \approx 200$ K in hexagonal MnNiGa.[14] We compared the lattice parameters (LPs) obtained from pressure- and temperature-dependent XRD (see Figure S4, S5 and Table S1, Supporting Information), which reveals that LP at 200 K ($\approx T_{SRT}$) are close to the LP at 0.7 GPa. This indicates that T_{SRT} or maximum density of biskyrmions can be stabilized at room temperature by using $P \approx 0.7$ GPa in hexagonal MnNiGa.

3. Conclusion

In summary, we have shown pressure-induced isostructural phase transition in the hexagonal MnNiGa using high-pressure synchrotron XRD analysis. The XRD pattern at ambient condition and AC-susceptibility measurements confirm the phase purity and magnetic phase transitions, respectively. The in situ high-pressure XRD data analysis up to 14 GPa reveals the continuous reduction of lattice parameters with nonlinearity above 4 GPa. The different compression rates of a-parameter (in-plane) and c-parameter (out-of-plane) indicate the anisotropic compression behavior. However, the hexagonal symmetry remains unchanged with pressure; the fitting of lattice volume

with pressure using second-order B–M equation of state reveals an isostructural phase transition around 4 GPa. A comparison of pressure and temperature-dependent lattice parameters suggests that SRT can be induced by ≈0.7 GPa pressure at room temperature. The present results open a new window for future investigation of pressure-tuning of skyrmions in the centrosymmetric MnNiGa and related systems.

4. Experimental Section

The polycrystalline sample of MnNiGa with nominal composition was prepared by the standard arc-melting method.[44] The appropriate quantity of each constituent element with minimum 99.99% purity was melted several times to get uniform composition. After melting, weight loss was found to be below 1%. The as-melted button-shaped ingot was taken in an evacuated quartz ampoule filled with argon gas and annealed at 800 °C for 6 days to get the homogeneous composition, and finally quenched in ice water mixture.[45] To check the chemical composition, energy-dispersive analysis of X-Rays (EDAX) characterization was performed using EVO-scanning electron microscope MA15/18 (ZEISS) equipped with an energy-dispersive spectroscopy detector (Model no. 51N1000-EDS System) in the backscattered electron mode. The average composition was found to be $Mn_{1.05}Ni_{0.95}Ga$, which corresponds to MnNiGa. The temperature-dependent AC-susceptibility data at a drive field 10 Oe for 333.33 Hz frequency was collected during the warming cycle on zero-field cooled sample using a superconducting quantum interference device-based magnetometer (MPMS, Quantum Design). The in situ high-pressure synchrotron X-Ray powder diffraction (XRD) measurements were carried out using X-rays with the wavelength of 0.49584 Å at Xpress beamline at Elettra, Trieste, Italy.[46] The data was collected up to 14 GPa using membrane-driven diamond anvil cell (DAC) for generating the pressure. The methanol–ethanol mixture in 4:1 ratio was employed for the pressure-transmitting medium. The pressure was monitored by the ruby fluorescence method wherein a few tiny ruby chips (≈5–10 μm) were included along with the powder sample in the DAC pressure chamber. The diffraction data were detected using PILATUS3S-6M detector. The 2D image was integrated into 1D (intensity vs 2θ) diffraction data using fit2D software. The temperature-dependent (300 to 15 K) laboratory source XRD patterns were collected using an 18 kW Cu-rotating-anode-based diffractometer attached with a closed-cycle He refrigerator.

The average crystal structure was determined by the Rietveld refinements[47] using the XRD data. The refinement was carried out using FULLPROF package[48] in the $P6_3/mmc$ space group (No. 194), considering all the atoms at special Wykoff positions, that is, Mn at 2*a* (0, 0, 0), Ni at 2*d* (1/3, 2/3, 3/4), and Ga at 2*c* (1/3, 2/3, 1/4).[14,16] The variation of unit cell volume with pressure was modeled with Birch–Murnaghan equation-of-state (B–M EoS)[39,40] using the EoSFit7-GUI software.[49] The B–M EoS is given as follows

$$P(V) = \frac{3B}{2}\left[\left(\frac{V_0}{V}\right)^{7/3} - \left(\frac{V_0}{V}\right)^{5/3}\right] \times \left\{1 + \frac{3}{4}(B' - 4)\left[\left(\frac{V_0}{V}\right)^{2/3} - 1\right]\right\} \quad (1)$$

In the aforementioned equation, V, V_0, B, and B' are volume, reference volume, bulk modulus, and pressure derivative of bulk modulus, respectively.[34] The second-order B–M EoS can be obtained by considering $B' = 4$ in the aforementioned equation.[50,51]

Supporting Information

Supporting Information is available from the Wiley Online Library or from the author.

Acknowledgements

S.S. is thankful to the Science and Engineering Research Board of India for financial support through the award of Ramanujan Fellowship (Grant no: SB/S2/RJN-015/2017) and UGC-DAE CSR, Indore, for financial support through the "CRS" Scheme. The major portions of this research were conducted using the light source of Elettra-Sincrotrone Trieste. BJ acknowledges the Xpress plus internal project of Elettra-Sincrotone Trieste. DST, Govt. of India, is acknowledged for support in performing the high-pressure diffraction measurements at the Xpress beamline of the Elettra (proposal no. 20205391).

Conflict of Interest

The authors declare no conflict of interest.

Data Availability Statement

The data that support the findings of this study are available from the corresponding author upon reasonable request.

Keywords

biskyrmions, hydrostatic compression, isostructural phase transition, magnetoelastic effect, spin reorientation transition

Received: February 15, 2022
Revised: April 4, 2022
Published online: April 28, 2022

[1] S. Mühlbauer, B. Binz, F. Jonietz, C. Pfleiderer, A. Rosch, A. Neubauer, R. Georgii, P. Böni, *Science* **2009**, *323*, 915.
[2] N. Nagaosa, Y. Tokura, *Nat. Nanotechnol.* **2013**, *8*, 899.
[3] L. Šmejkal, Y. Mokrousov, B. Yan, A. H. MacDonald, *Nat. Phys.* **2018**, *14*, 242.
[4] P. K. Rout, P. P. Madduri, S. K. Manna, A. K. Nayak, *Phys. Rev. B* **2019**, *99*, 094430.
[5] Z.-X. Li, Z. Wang, Y. Cao, H. Zhang, P. Yan, *Phys. Rev. B* **2021**, *103*, 054438.
[6] C. Sürgers, G. Fischer, P. Winkel, H. V. Löhneysen, *Nat. Commun.* **2014**, *5*, 1.
[7] C. D. O'Neill, A. S. Wills, A. D. Huxley, *Phys. Rev. B* **2019**, *100*, 174420.
[8] F. Jonietz, S. Mühlbauer, C. Pfleiderer, A. Neubauer, W. Münzer, A. Bauer, T. Adams, R. Georgii, P. Böni, R. A. Duine, *Science* **2010**, *330*, 1648.
[9] T. Schulz, R. Ritz, A. Bauer, M. Halder, M. Wagner, C. Franz, C. Pfleiderer, K. Everschor, M. Garst, A. Rosch, *Nat. Phys.* **2012**, *8*, 301.
[10] T. Yokouchi, N. Kanazawa, A. Tsukazaki, Y. Kozuka, M. Kawasaki, M. Ichikawa, F. Kagawa, Y. Tokura, *Phys. Rev. B* **2014**, *89*, 064416.
[11] C. H. Back, V. Cros, H. Ebert, K. Everschor-Sitte, A. Fert, M. Garst, T. Ma, S. Mankovsky, T. Monchesky, M. V. Mostovoy, *J. Phys. D: Appl. Phys.* **2020**, *53*, 363001.
[12] X. Xiao, L. Peng, X. Zhao, Y. Zhang, Y. Dai, J. Guo, M. Tong, J. Li, B. Li, W. Liu, *Appl. Phys. Lett.* **2019**, *114*, 142404.
[13] X. Yu, Y. Tokunaga, Y. Kaneko, W. Zhang, K. Kimoto, Y. Matsui, Y. Taguchi, Y. Tokura, *Nat. Commun.* **2014**, *5*, 3198.
[14] W. Wang, Y. Zhang, G. Xu, L. Peng, B. Ding, Y. Wang, Z. Hou, X. Zhang, X. Li, E. Liu, *Adv. Mater.* **2016**, *28*, 6887.
[15] L. Peng, Y. Zhang, W. Wang, M. He, L. Li, B. Ding, J. Li, Y. Sun, X.-G. Zhang, J. Cai, *Nano Lett.* **2017**, *17*, 7075.

[16] G. Xu, Y. You, J. Tang, H. Zhang, H. Li, X. Miao, Y. Gong, Z. Hou, Z. Cheng, J. Wang, *Phys. Rev. B* **2019**, *100*, 054416.
[17] Y. You, G. Xu, J. Tang, Y. Gong, F. Xu, *Intermetallics* **2019**, *106*, 88.
[18] A. Singh, A. Senyshyn, H. Fuess, T. Chatterji, D. Pandey, *Phys. Rev. B* **2011**, *83*, 054406.
[19] D. Saha, R. Ranjan, D. Swain, C. Narayana, T. N. G. Row, *Dalton Trans.* **2013**, *42*, 7672.
[20] M. Plumer, M. Walker, *J. Phys. C: Solid State Phys.* **1982**, *15*, 7181.
[21] Y. Hu, B. Wang, *New J. Phys.* **2017**, *19*, 123002.
[22] Y. Nii, T. Nakajima, A. Kikkawa, Y. Yamasaki, K. Ohishi, J. Suzuki, Y. Taguchi, T. Arima, Y. Tokura, Y. Iwasa, *Nat. Commun.* **2015**, *6*, 1.
[23] A. Chacon, A. Bauer, T. Adams, F. Rucker, G. Brandl, R. Georgii, M. Garst, C. Pfleiderer, *Phys. Rev. Lett.* **2015**, *115*, 267202.
[24] J. Chen, W. Cai, M. Qin, S. Dong, X. Lu, X. Gao, J.-M. Liu, *Sci. Rep.* **2017**, *7*, 1.
[25] L. Deng, H.-C. Wu, A. P. Litvinchuk, N. F. Yuan, J.-J. Lee, R. Dahal, H. Berger, H.-D. Yang, C.-W. Chu, *Proc. Natl. Acad. Sci.* **2020**, *117*, 8783.
[26] L. J. Bannenberg, R. Sadykov, R. M. Dalgliesh, C. Goodway, D. L. Schlagel, T. A. Lograsso, P. Falus, E. Lelièvre-Berna, A. O. Leonov, C. Pappas, *Phys. Rev. B* **2019**, *100*, 054447.
[27] K. Shibata, J. Iwasaki, N. Kanazawa, S. Aizawa, T. Tanigaki, M. Shirai, T. Nakajima, M. Kubota, M. Kawasaki, H. Park, *Nat. Nanotechnol.* **2015**, *10*, 589.
[28] S. Pal, P. Malavi, S. Chaturvedi, S. Das, S. Karmakar, D. Muthu, U. V. Waghmare, A. Sood, *Phys. Rev. B* **2020**, *102*, 214107.
[29] S. Bhattacharjee, K. Taji, C. Moriyoshi, Y. Kuroiwa, D. Pandey, *Phys. Rev. B* **2011**, *84*, 104116.
[30] V. Rajaji, U. Dutta, P. Sreeparvathy, S. C. Sarma, Y. Sorb, B. Joseph, S. Sahoo, S. C. Peter, V. Kanchana, C. Narayana, *Phys. Rev. B* **2018**, *97*, 085107.
[31] G. Li, Y. Li, M. Zhang, Y. Ma, Y. Ma, Y. Han, C. Gao, *RSC Adv.* **2014**, *4*, 42523.
[32] T. Kanomata, K. Shirakawa, T. Kaneko, *Phys. Status Solidi A* **1986**, *97*, K149.
[33] A. K. Srivastava, P. Devi, A. K. Sharma, T. Ma, H. Deniz, H. L. Meyerheim, C. Felser, S. S. Parkin, *Adv. Mater.* **2020**, *32*, 1904327.
[34] S. N. Gupta, A. Singh, S. Sarkar, D. Muthu, S. Sampath, U. Waghmare, A. Sood, *Phys. Rev. B* **2020**, *101*, 035123.
[35] F. Occelli, D. L. Farber, J. Badro, C. M. Aracne, D. M. Teter, M. Hanfland, B. Canny, B. Couzinet, *Phys. Rev. Lett.* **2004**, *93*, 095502.
[36] Q. Liu, X. Yu, X. Wang, Z. Deng, Y. Lv, J. Zhu, S. Zhang, H. Liu, W. Yang, L. Wang, H. Mao, G. Shen, Z.-Y. Lu, Y. Ren, Z. Chen, Z. Lin, Y. Zhao, C. Ji, *J. Am. Chem. Soc.* **2011**, *133*, 7892.
[37] S. Karmakar, S. M. Sharma, P. V. Teredesai, A. K. Sood, *Phys. Rev. B* **2004**, *69*, 165414.
[38] M. Mitrano, M. Mitrano, B. Maroni, C. Marini, M. Hanfland, B. Joseph, P. Postorino, L. Malavasi, *Phys. Rev. B* **2012**, *85*, 184108.
[39] F. Murnaghan, *Proc. Natl. Acad. Sci. U. S. A.* **1944**, *30*, 244.
[40] F. Birch, *Phys. Rev.* **1947**, *71*, 809.
[41] S. B. Pillai, B. Joseph, D. Upadhyay, C. Marini, P. K. Jha, *J. Phys. Chem. C* **2021**, *125*, 2785.
[42] R. Vilaplana, D. Santamaría-Pérez, O. Gomis, F. Manjón, J. González, A. Segura, A. Muñoz, P. Rodríguez-Hernández, E. Pérez-González, V. Marín-Borrás, *Phys. Rev. B* **2011**, *84*, 184110.
[43] A. Polian, M. Gauthier, S. M. Souza, D. M. Trichês, J. C. de Lima, T. A. Grandi, *Phys. Rev. B* **2011**, *83*, 113106.
[44] B. Holt, J. Diaz, J. Huber, C. A. Luengo, *Rev. Bras. Fis.* **1978**, *8*, 155.
[45] L. A. Turnbull, M. T. Birch, A. Laurenson, N. Bukin, E. O. Burgos-Parra, H. Popescu, M. N. Wilson, *ACS Nano* **2020**, *15*, 387.
[46] P. Lotti, S. Milani, M. Merlini, B. Joseph, F. Alabarse, A. Lausi, *J. Synchrotron Radiat.* **2020**, *27*, 222.
[47] R. A. Young, *The Rietveld Method*, Oxford University Press, Oxford **1993**.
[48] J. Rodriguez-Carvajal, *Version, April* **2008**.
[49] J. Gonzalez-Platas, M. Alvaro, F. Nestola, R. Angel, *J. Appl. Crystallogr.* **2016**, *49*, 1377.
[50] F. Rivadulla, M. Banobre-Lopez, C. X. Quintela, A. Pineiro, V. Pardo, D. Baldomir, M. A. Lopez-Quintela, J. Rivas, C. A. Ramos, H. Salva, J. S. Zhou, J. B. Goodenough, *Nat. Mater.* **2009**, *8*, 947.
[51] B. Zhang, C. An, X. Chen, Y. Zhou, Y. Zhou, Y. Yuan, C. Chen, L. Zhang, X. Yang, Z. Yang, *Chin. Phys. B* **2021**, *30*, 076201.